THE JOURNAL OF PHYSICAL CHEMISTRY C
A JOURNAL OF THE AMERICAN CHEMICAL SOCIETY

pubs.acs.org/JPCC

Article

Charge Transfer in Molecular Cocrystals: A Plane Wave vs Localized-Orbital View—Structural Information Obtained from Calculated Raman and IR Phonons

Fabio Biffoli,[○] Davide Vanossi,[○] Elisabetta Venuti, Tommaso Salzillo, Marco Bonechi, Massimo Innocenti, Marco Pagliai, and Claudio Fontanesi*

Cite This: *J. Phys. Chem. C* 2024, 128, 14046−14055

Read Online

ACCESS | Metrics & More | Article Recommendations | Supporting Information

ABSTRACT: This article aims at laying the foundation for the development of electronic structure−property relationships in the field of charge-transfer (CT) organic semiconductors by studying the low-frequency phonon response of donor−acceptor (DA) compounds. In this article, it is shown and discussed how and why phonon frequencies and their delocalization depend on the interplay between single-molecule properties and crystal structures. These results are obtained by combining results from state-of-the-art quantum−mechanical calculations, carried out within both localized orbitals and a plane wave paradigm, with simple classical models. CT compounds obtained from perylene (Pery) as the donor and F*n*TCNQ (n = 0, 4) as the acceptors are considered.

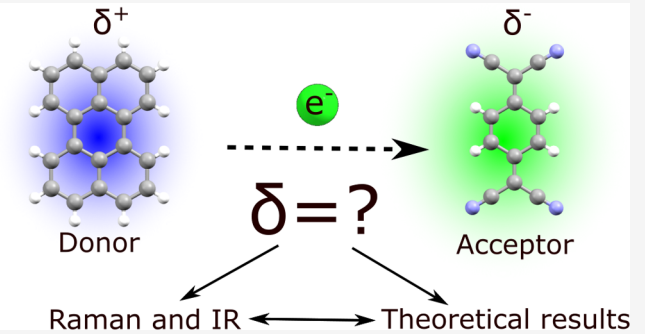

INTRODUCTION

Following the seminal work of Heeger, MacDiarmid, and Shirakawa on molecularly doped conjugated polymers, scientific research based on the development of hydrocarbon-based semiconducting materials drove the development of the so-called "organic electronics" field of research activity.[1−5] In particular, semiconducting polymers are at present mainly employed in cheap and easily assembled thin-film transistors,[6] light-emitting materials,[7] and dye-sensitized solar cells (DSSCs).[8] From a purely application point of view, maybe the most effective manifestation of organic electronics in the impact on everyday life is the production of screen and touch-screen devices for the display of monitors and smartphones. In this context, conjugated sulfur-containing aromatic systems, i.e., polythiophenes, remain the most popular choices for the preparation of organic electronic materials, in which (i) they are typically good donors and (ii) the preferentially planar geometrical arrangement and the presence of 3p orbitals on sulfur atoms enable an efficient intermolecular orbital overlap. These characteristics make them very good candidates as donors in binary charge-transfer (CT) complexes.[9] Although CT complexes have long been known, their potentials as electronic materials have not been noted until relatively recently, despite the capability to fine-tune their electric properties depending on heteroatoms and substituents.[10] Previous reports indicated that binary CT complexes show high conductivity and other promising optoelectronic properties, such as ambipolar transport and photoconductivity.[11] The electronic properties of CT complexes have also been exploited to develop a wide variety of colorimetric sensors based on the increasing number of characteristic absorption bands.[12] A comprehensive review of the experimental and theoretical research on this topic was proposed by Pramanik et al.[13] In the field of CT complexes, molecular crystals represent an important class of materials because the tunability of their properties is strictly dependent on their crystalline structure.[10,14,15]

Molecular crystals are ordered packings of molecules that are discrete physical entities that characterize the solids. It can be seen that forces determining the packing in molecular crystals are much weaker than those of ionic or covalent chemical bonds.[16,17] The physical nature of such weaker intermolecular forces can be used to characterize the crystal itself and its properties.[18] Among the various types of molecular solids, organic charge-transfer crystals have attracted significant research attention due to their wide range of potential applications in organic optoelectronic devices,[19] organic magnetic devices, organic energy devices, etc. In this type of solid, donor−acceptor interactions occur between "planar" donor (D) and acceptor (A) molecules packed in an infinite

Received: May 26, 2024
Revised: August 1, 2024
Accepted: August 1, 2024
Published: August 10, 2024

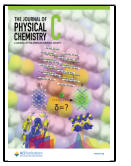

Downloaded via UNIV DEGLI STUDI DI MODENA on December 18, 2024 at 17:30:39 (UTC).
See https://pubs.acs.org/sharingguidelines for options on how to legitimately share published articles.

ACS Publications
© 2024 American Chemical Society

https://doi.org/10.1021/acs.jpcc.4c03470
J. Phys. Chem. C 2024, 128, 14046−14055

arrangement; to this end, a crucial role is related to the energy difference of the HOMO (D) and the LUMO (A) orbitals.

The Born−Oppenheimer electronic ground state of such systems is partially ionic in nature, and the degree of CT is largely responsible for the resulting properties of the crystals.[20] It is worthwhile to emphasize that, in systems with long-range crystalline order, not only the energy difference between the HOMO and the LUMO is important in determining the value of CT, but also the electronic coupling between these frontier orbitals plays a crucial role.[21,22] The degree of CT can be, for example, estimated by single-crystal XRD[23] by calculating variations in bond lengths. However, in this study, we used vibrational spectroscopy (IR and Raman) to estimate the value of CT for organic charge-transfer crystals; it is in fact widely recognized that charge- transfer interactions influence some vibrational modes of both donor and acceptor molecules.[24,25] In parallel, theoretical studies were conducted to validate and predict experimental CTs from vibrational spectra; despite the importance of the estimation of CT, these measurements, both from an experimental and a computational point of view, led to conflicting results.[14,20,26,27] This review aims to delve into the theoretical aspects of determining the CT by validating and suggesting a novel and robust workflow to obtain reliable CT values for molecular crystals by an in silico approach. The degree of CT and the influence of the level of theory on its estimation were benchmarked within density functional theory (DFT), testing both localized orbitals (LOs) and plane waves (PWs), and investigating the interaction between these and different population analyses. Perylene (Pery) Fn-7,7,8,8-tetracyanoquinodimethane (F*n*TCNQ) cocrystals were selected as prototypical organic charge-transfer crystals as they have been extensively studied and characterized and still represent a system of interest because of their variety and fine-tuning possibilities.[28−34] The CT in molecular crystals is strictly linked to the electronic band structure, making the study of this variable important for electrochemical experiments because bandgaps can be accessed via cyclic voltammetry, and a robust protocol to theoretically verify experimental results is necessary.[27,35,36]

EXPERIMENTAL SECTION

CT crystals were prepared following a previously reported procedure by Salzillo et al.[20] by a physical vapor transport method. THz-IR (or Far-IR) measurements were performed with an in-house setup based on a Bomem DA8 interferometer with a maximum spectral resolution of 0.004 cm^{-1} working in a final vacuum in the range of 10^{-4} mbar and equipped with a Globar source cooled water, Mylar Hyperspectral beamsplitter and a DTGS detector. The signal was collected in transmission mode with the samples previously dispersed in polyethylene powder (Sigma-Aldrich (UHMW PE), powder, mean particle size: 150 μm) and pressed at room temperature in pellets. The pellet is prepared by dispersing about 1 mg of the sample in crystal form and mixing it with 60 mg of polyethylene powder using an agate mortar to achieve the homogenity. Each spectrum is the result of 9999 scans with 2 cm^{-1} spectral resolution, and as a background, a KBr spectrum recorded under the same conditions has been used. THz-Raman (or low-frequency Raman) measurements have been performed with a Horiba Jobin Yvon T64000 triple grating spectrometer working in double subtractive + single additive configuration under ambient conditions. The excitation laser line was from a Krypton ion gas laser (Coherent Innova 90C) tuned at 647.1 nm and power-modulated using neutral optical density filters to obtain about 1 mW on the sample to avoid its degradation. Each spectrum was recorded with 100× objective, integrating 240 s and averaging 6 spectra. For each crystal, at least 6 independent measurements were recorded to ensure the homogeneity of the sample. The calibration of the triple spectrometer was performed with a narrow neon emission lamp.

Calculation Details. Projector-augmented wave (PAW) calculations with periodic boundary conditions (PBCs) were performed with the VASP 5.4.4 program,[37,38] selecting the h_GW family of default PAW pseudopotentials[39,40] and an energy cutoff of 910 eV. Dispersion-corrected density functional theory (DFT-D) was employed with the PBE[41] exchange and correlation functional coupled with the D3(BJ) empirical correction to account for dispersion interaction.[42] Geometries and cell parameters were optimized using the conjugate-gradient method starting from the experimental X-ray results[20] (the experimental geometries are attached as F0TCNQPerylene_1-1.cif and F4TCNQPerylene_1-1.cif files in the Supporting Information). For this work, the α-polymorph with a donor−acceptor stoichiometry of 1:1 was considered for both species, setting with the $P2_1/c$ space group as symmetry constrain for Pery:TCNQ and p-1 for Pery:F4TCNQ. For both species, the k-points were Γ-centered and automatically generated. For Pery:F4TCNQ, a 6 × 6 x 4 Monkhorst sampling was used, and then, a 5 × 3 × 3 sampling was used Pery:TCNQ. Frequency calculations were performed at Γ, thanks to the Phonopy package[43] with a finite difference approach (0.01 Å displacements), employing VASP 5.4.4 as the force calculator. IR intensities and Raman activities were evaluated, thanks to the Phonopy-spectroscopy framework.[44] A 2 × 1 × 1 supercell was needed for the Pery:F4TCNQ crystal to ensure convergence. The electronic structures of the dimers were also evaluated using LOs, in the Gaussian 16[45] environment at the DFT-D level, implementing again D3(BJ) empirical dispersions. Different population analyses were benchmarked to obtain the following atomic charges: Mulliken, Bader, and DDEC6. DDEC6 charges were evaluated with chargemole[46] both for LO and PAW calculations. Mulliken charges for LOs were obtained from Gaussian 16; for PAWs, instead, the LOBSTER program was used, setting pbeVaspFit2015 as the auxiliary basis set.[47] Finally, Bader charges were processed with Henkelman's group code[48,49] for PAWs and with Multiwfn[50] for LOs. The influences of different basis sets and functionals on population analyses were tested by varying both in LO calculations. We selected CAM-B3LYP[51] as our high level hybrid functional and cc-pVTZ[52] as the reference basis set: various exchange and correlation functionals (BLYP,[53] B3LYP,[54] PBE, and PBE0[55]) against the CAM-B3LYP(D3BJ)/cc-pVTZ standard. The effect of the basis set extension and the influence of polarization and diffuse functions were also tested by employing the following basis sets in conjunction with the CAM-B3LYP functional: 6-31G,[56] 6-31G(d),[56,57] 6-31+G,[56,58] 6-31+G(d),[56−58] 6-311G-(2d,2p),[57,59] 6-311++G(2d,2p),[57−59] 6-311++G-(3df,3pd),[57−59] cc-pVDZ,[60] aug-cc-pVDZ,[52,60] cc-pVTZ, and aug-cc-pVTZ.[52] The theoretical CT was determined by the sum of net atomic charges over a Pery molecule.

RESULTS AND DISCUSSION

In CT complexes, the central question is represented by the determination of the amount of charge transferred between the

https://doi.org/10.1021/acs.jpcc.4c03470
J. Phys. Chem. C 2024, 128, 14046−14055

Chart 1. Optimized Crystal Structure at the PBE(D3BJ)/PAW Level of A) Triclinic Pery:F4TCNQ Stoichiometry 1:1 with *p*-1 as the Space Group and B) Monoclinic Pery:TCNQ, Stoichiometry 1:1 with $P2_1/c$ as the Space Group

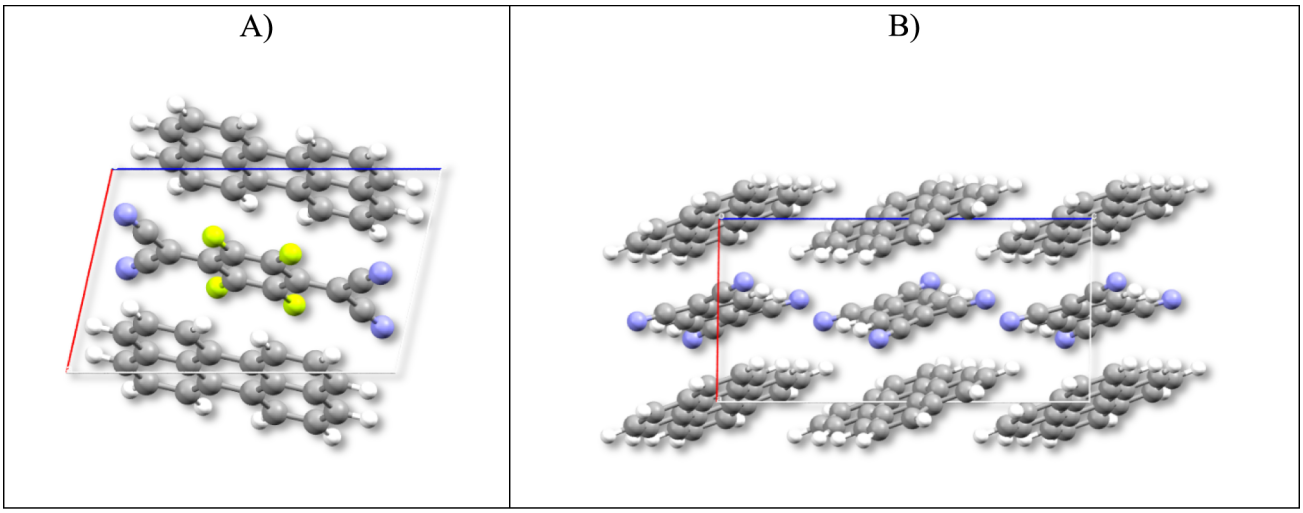

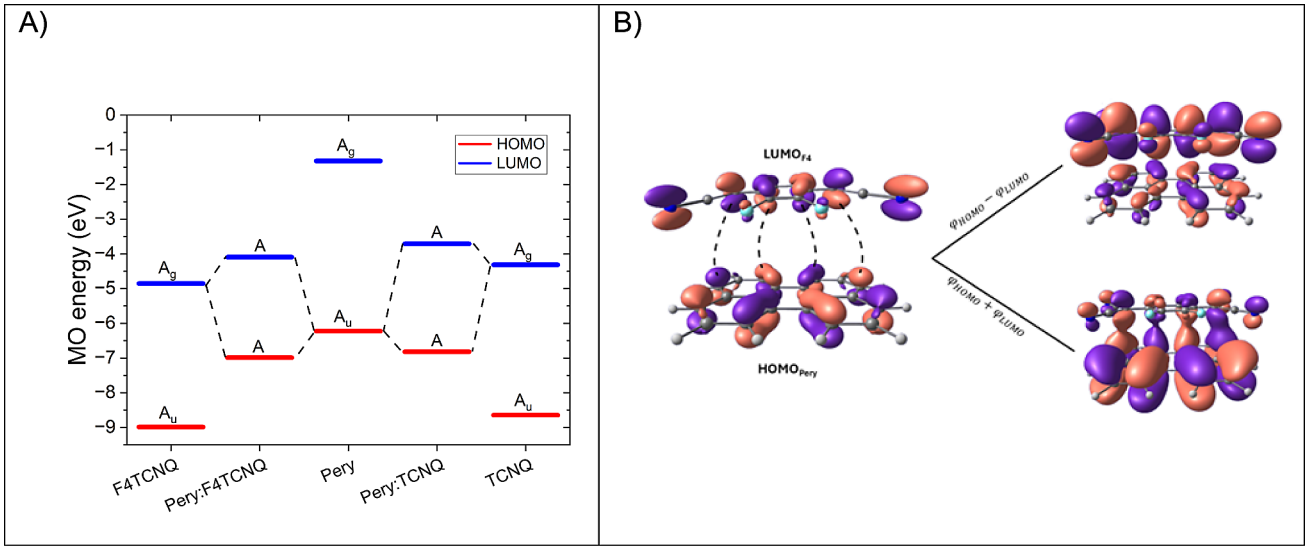

Figure 1. A) Pery, TCNQ, and F4TCNQ frontier orbital correlation diagram at the CAM-B3LYP(D3BJ)/cc-pVTZ level of the theory. The diagram also shows the frontier orbitals of Pery:TCNQ and Pery:F4TCNQ CT complexes. The calculation was performed extracting the dimer geometry from the optimized structures after PAW calculations (with PBC). B) Constructive and destructive combination of frontier orbitals of Pery and F4TCNQ; it can be seen how the inversion centers of donors and acceptors are not aligned to obviate the orthogonality between the Pery HOMO (A_u) and F4TCNQ LUMO (A_g).

donor and acceptor. Indeed, the crux is to devise a strategy that allows for reliable quantitative estimation, both experimentally as well as theoretically.[31,61−63] Pery:F4TCNQ with a 1:1 stoichiometry CT cocrystal constitutes an interesting benchmark for any theoretical approach; in that, from the analysis of IR spectra, a charge transfer value of 0.29 electrons is obtained experimentally with the formation of positively charged Pery.[20] We selected F*n*TCNQ (n = 0, 4) from the whole series as there is no intrinsic disorder due the asymmetry of the acceptor, as for n = 1, 2, 3, making these species more suitable for a systematic theoretical study. Chart 1 shows the optimized crystal structure at the PBE(D3BJ)/PAW level (the optimized geometries are attached as F0TCNQPerylene_1-1_opt.cif and F4TCNQPerylene_1-1_opt.cif files in the Supporting Information). A comparison of the experimental and optimized lattice parameters is reported in Table S1 for both species, underlining good agreement between the experimental and theoretical results.

Figure 1 displays the frontier orbital correlation diagram for the isolated pristine species Pery, TCNQ, and F4TCNQ together with the relevant 1:1 stoichiometry CT complexes. In that, the driving force of the CT process is often rationalized considering that the LUMO energy of the acceptor has to be near in energy with respect to that of the HOMO of the donor. Note that both the donors and acceptors undergo a decrease in electronic state symmetry, passing from D_{2h} (isolated molecule) to C_i (in the crystal, concerning the symmetry of the elementary cell). In order to form the donor−acceptor complex, the two species must be arranged in a staggered manner, further lowering the symmetry of the dimer to C_1. This disposition minimizes the orthogonality between the HOMO of the donor (A_g) and the LUMO of the acceptor (A_u). This geometry reduces the need for charge transfer

https://doi.org/10.1021/acs.jpcc.4c03470
J. Phys. Chem. C 2024, 128, 14046−14055

between the LUMO and the HOMO−1 reported in the literature for similar cases.[64] This can be observed in Figure 1B, where the LUMO and HOMO of F4TCNQ and Pery are combined to give constructive and destructive patterns, respectively, highlighting how the two species are positioned to avoid the orthogonality of the considered molecular orbitals.

Figure 2 gives a single-glance comparison of the theoretical and experimental IR spectra, the shift in the energy of the bands labeled with an asterisk, ("*", in Figure 2), is used for estimating experimentally the CT. It was accomplished by comparing the corresponding vibrational bands of the neutral acceptor molecule. In this case F4 (reference vibrational energy values for the neutral F4 and F0 acceptor compounds are reported in Table S2). Overall, the calculated pattern shows a rather good match with the data reported in the literature. This was verified also taking into account the differences in the experimental IR spectra due to crystal anisotropic factors (orientation concerning the direction of the incident radiation), as already discussed in detail in ref 20. The agreement between the calculated (plane wave) and experimental IR spectra strongly suggests the agreement between the optimized structure and effective crystal geometry, allowing us to proceed further in the calculation of the charge transfer, with 0.29 electrons as a reference value. It has to be noted that, vibrational frequencies reported in Figure 2 are scaled by a factor of 1.02 (which will be discussed lately in the manuscript), which was determined following an error minimization procedure: the calculation of the root-mean square deviation (RMSD) between theoretical data and experimental values in the near-IR region concerning experimental data of IR spectra available for both the Pery:F0 (1:1 stoichiometry) and Pery:F4 (1:1).[14,20] This was accomplished by performing a linear regression between the marked ("*") bands and modes 130 and 133 for Pery:F4 (1:1) and mode 256 for Pery:F0 (1:1). Unscaled frequencies are reported in Table S3 and Supporting Information.

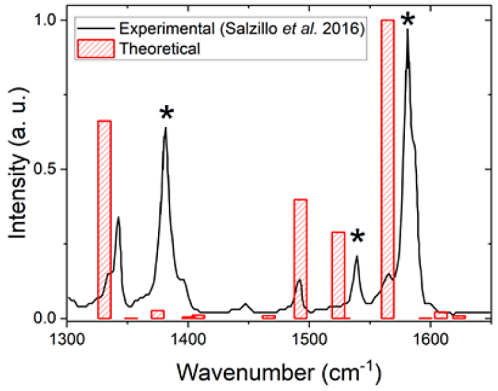

Figure 2. IR spectra of the Pery:F4TCNQ CT complex, 1:1 stoichiometry. The black line is the experimental spectrum.[20] Red bars are the theoretical spectra, calculated at the PBE(D3BJ)/PAW (plane wave) level of the theory. Asterisks labels, "*", underline bands that are considered for evaluating the experimental CT (see the text for details).

Figure 3 shows the charge transfer values of the Pery:F4 complex as a function of both the levels of the theory and as a function of different approaches used in this work (Mulliken, Bader, and DDEC6) to calculate localized atomic net charge values.

It must be noted that (i) there is a strong influence of the calculated CT value as a function of the quantum mechanical-based paradigm, i.e., "localized orbitals", LO, vs "plane wave", PW Hamiltonians, and (ii) the strategy/scheme of electron density partition also has a rather strong influence; the latter is an already well-known point in LO calculations where Löwdin and Mulliken "net charges" are recognized to yield substantially different results by varying the basis set, as they depend explicitly on the coefficients of the LCAO expansion. Indeed, this result seems especially evident for the Bader scheme population analysis, which seems to overestimate the ionicity of the system, as also reported in the literature.[65,66] For instance, Bader values obtained in the LO paradigm appear rather in line with the experimental 0.29 electron values (red dotted line in Figure 3), while PW values appear as rather unreliable, with about 50% error compared with the experimental value. Hence, on the basis of the results reported in Figure 3, the value of 0.29 electrons, obtained from the elaboration of experimental IR results, is in general agreement with the theoretical results, especially with the one obtained at the higher level of theory (CAM-B3LYP(D3BJ)/cc-pVTZ). This saves for the Bader charges, which yield values substantially different from the experimental estimation and thus appear not suitable for evaluating CT values in molecular

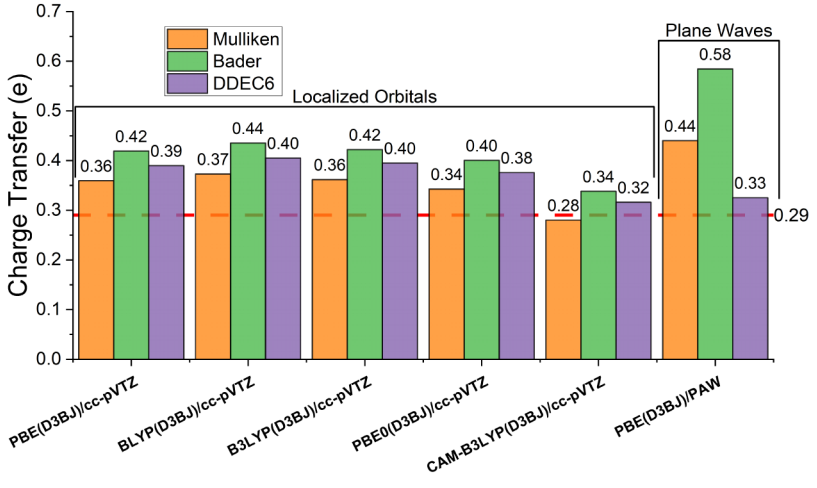

Figure 3. Calculated CT of Pery-F4_1:1 at various levels of theory employing Mulliken, Bader, or DDEC6 population analysis.

https://doi.org/10.1021/acs.jpcc.4c03470
J. Phys. Chem. C 2024, 128, 14046−14055

crystals, as the overestimated ionicity bias appropriate for the population analysis is compensated only by the long-range corrected functional. Despite that, Bader analysis is widely used in the field of PW calculations and has already been exploited to define the theoretical CT of similar systems, leading to comparable results;[27] therefore, considering the results obtained from this benchmark, the use of the Bader electron density decomposition to evaluate CT of molecular crystals from calculated electronic densities with PW is deplorable. Comparing the LO and PW results shows that the main problem is the use of pseudopotentials that localize the core electrons on the center of mass of atoms, introducing a nonignorable error. The Mulliken net-charge scheme seems to work more efficiently when compared to Bader charges for PW for the same reason, as the LOBSTER protocol involves treating the core part with an auxiliary basis set, thus limiting the error introduced by pseudopotentials; in the same fashion, the DDEC6 method aims to correct the error due to the use of pseudopotentials by exploiting a test electron density fitted to reproduce LO calculations. Moreover, the best performing exchange and correlation functional is CAM-B3LYP, accounting for the minor ionicity and giving CTs of 0.28, 0.34, and 0.32 electrons for Mulliken, Bader, and DDEC6, respectively (experimental value: 0.29 e). This performance is due to a more reliable reproduction of π-polarizability; the latter is a fundamental aspect in modeling CT π-complexes such as the system under examination.[67] The influence of the basis set to the CT value is also investigated by benchmarking the impact of diffuse and polarization functions; all the results are reported in Table 1. As expected, the Mulliken population analysis does not converge approaching the complete basis set, with a nonphysical value of 0.02 electrons for the most extended basis set tested (aug-cc-pVTZ) and an RMSD of 0.44 electrons. Both Bader and DDEC6 schemes perform well with an RMSD of, respectively, 0.17 and 0.12 electrons and maintaining the trend observed in Figure 3 with the Bader charges overestimating the ionicity in comparison to DDEC6. Another important observation is a major increase in ionicity given by the addition of diffuse functions for Pople's basis sets. The same effect was observed for double-ζ Dunning's basis set but not for its triple-ζ counterpart, with a change of only 0.01 electrons passing from cc-pVTZ to aug-cc-pVTZ. On the other hand, the effect of polarization functions seems to be minor, with a negligible difference passing from 6 to 31G, 6-31+G, and 6-311++G(2d,2p) to 6-31G(d), 6-31+G(d), and 6-311++G(3df,3pd).

Table 1. Charge Transfer (CT) of Pery-F4_1:1 Evaluated by Varying the Basis Set and Population Analysis; the RMSD Related to the Experimental Value is also Reported

level of theory (CAM-B3LYP(D3BJ)/x)	Mulliken CT (e)	Bader CT (e)	DDEC6 CT (e)
6-31G	0.30	0.33	0.31
6-31+G	0.12	0.36	0.35
6-31G(d)	0.29	0.32	0.30
6-31+G(d)	0.51	0.36	0.34
6-311G(2d,2p)	0.27	0.33	0.31
6-311++G(2d,2p)	0.14	0.35	0.33
6-311++G(3df,3pd)	0.17	0.34	0.33
cc-pVDZ	0.26	0.31	0.29
aug-cc-pVDZ	0.46	0.35	0.33
cc-pVTZ	0.28	0.34	0.32
aug-cc-pVTZ	0.02	0.34	0.33
RMSD	0.47	0.17	0.12

Furthermore, to define the CT of Pery:F0, the DDEC6 population analysis was selected for both the LO and PWs as it was the only reliable charge transfer value for PW Hamiltonian, and it has a lower basis set dependence for LO. In addition, as already observed in Figure 3, DDEC6 CTs were noticeably better than the ones evaluated with Bader population analysis for all the functionals tested, and the good agreement with the experimental value of Mulliken CTs is only ascribed to the choice of the basis set.

Figure 4 shows the IR and Raman spectra for the Pery:F0 CT complex (1:1 stoichiometry). Figure 4A shows a tight comparison between the IR experimental and theoretical (calculated at the PBE(D3BJ)/PAW level of the theory) outcomes, concerning in particular, the typical crystal fingerprint wavelength region; a reasonable agreement is found between the experimental and theoretical results. On the contrary, the comparison between experimental (estimated CT 0.0 electrons) and theoretical Raman spectra in ref. 26, reported in Figure S1, shows a rather substantial difference. Indeed, due to the symmetry of the crystal, which is characterized by the presence of an inversion center, the correct frequency match of IR active modes should also bring to a correct match for the Raman spectrum. This is probably related to the polarization of Raman spectra reported in ref 26 which brings a dependency between laser polarization and crystal orientation (that is not taken into account in the simulation, as the frequencies and intensities were evaluated at Γ). This could foreshadow that the reported CT of 0 electrons, i.e., no charge transfer, could not be correct. Thus, to verify this hypothesis, in this work, three different Raman spectra obtained at different crystal orientations (Figure S2) were summed and compared to the theoretical results (Figure 4B). Despite still not perfect, we achieved a better agreement between the theoretical and experimental data (in comparison with ref. 26 and polarization averaged spectra is also reported in Figure S1). The frequencies of the theoretical Raman spectrum reported in Figure 4B were scaled to 0.98. Which is a typical scaling factor recommended in the case of PBE calculations[68] (please note that unscaled frequencies are reported in Table S4). All experimental Raman intensities were converted into Raman activities using eq 1[69−71]

$$A_i = I_i \frac{\nu_i\left(1 - \exp\left(-\frac{hc\nu_i}{kT}\right)\right)}{(\nu_0 - \nu_i)^4} \quad (1)$$

k, c, and h are fundamental constants, ν_o is the laser frequency (cm^{-1}), ν_i is the vibrational frequency (cm^{-1}) of the ith normal mode, T is the temperature (K), and f is a suitably chosen common normalization factor for all peak intensities.

Concerning the calculated CT value for the Pery:F0 complex, Table 2 shows DDEC6 CT values calculated at the PBE(D3BJ)/PAW and CAM-B3LYP(D3BJ)/cc-pVTZ levels of the theory, which indeed are in close agreement with the experimental CT reported by Henderson[14] of 0.15 ± 0.05 electrons obtained both from IR spectroscopy and HOSE analysis.[72]

Figure 5 shows a comparison between the calculated spectrum and one already published in the literature;[14,20] the band marked ("*") was exploited to determine the experimental CT. The calculated frequencies are scaled by

https://doi.org/10.1021/acs.jpcc.4c03470
J. Phys. Chem. C 2024, 128, 14046−14055

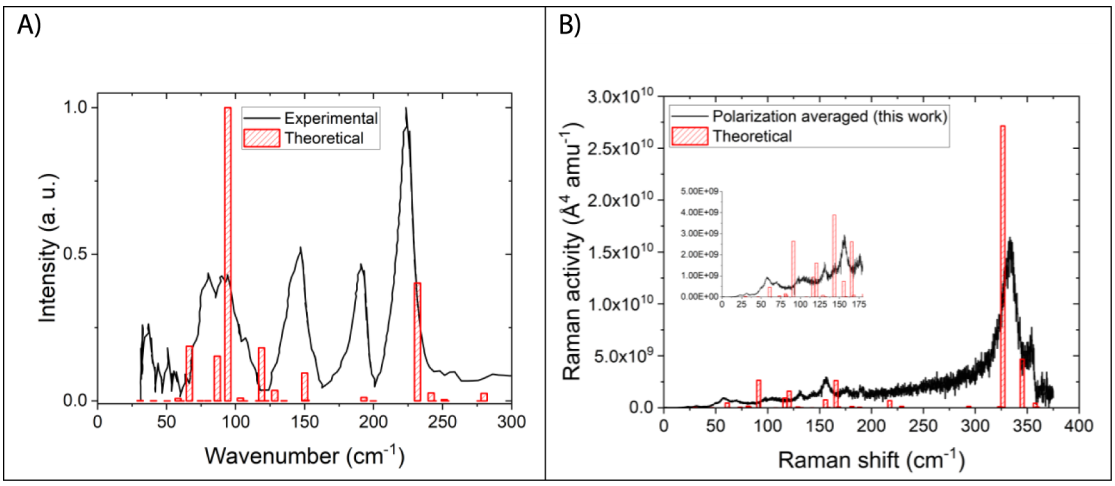

Figure 4. Pery:F0 CT crystal: A) IR spectra and B) Raman spectra. Theoretical spectra are calculated at the PBE(D3BJ)/PAW level of the theory.

Table 2. Calculated CT Values and DDEC6 for Pery-F0_1:1: PBE(D3BJ)/PAW and CAM-B3LYP(D3BJ)/cc-pVTZ[a]

level of theory	DDEC6 CT (e)	experimental value by Henderson et al.[14] (e)	experimental value by Vermeulen et al.[26] (e)
CAM-B3LYP(D3BJ)/cc-pVTZ[†]	0.16	0.15	0
PBE(D3BJ)/PAW[‡]	0.23		

[†]localized orbital basis set. [‡]plane wave basis set. [a]Thus, confirming a CT value equal to 0.15 ± 0.05 electrons, it is important to notice how the result of the PW basis set is slightly upper the experimental error. This hints at how better the results for low CT systems are given by extracting the D−A dimer and processing it with an LO basis set.

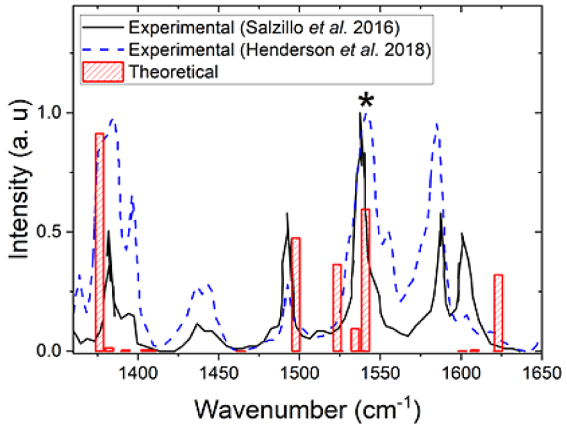

Figure 5. Pery:F0 CT crystal (1:1 stoichiometry), experimental IR spectra from refs 14 and 20 Red bars are the theoretical spectrum calculated at the PBE(D3BJ)/PAW level of the theory. The band indicated by the asterisk, "*", is considered for the experimental estimation of the CT value.

1.02 as shown in Figure 2 (unscaled frequencies are reported in Table S4).

Again, the charge transfer value determined by using a pseudopotential basis set yields a higher result than the experimental one, likely due to the overestimation of the ionicity of the system as a result of the use of pseudopotentials for core electrons. Charge-sensitive intramolecular modes of F0 and F4 are red-shifted in comparison to the experimental values. Hence, comparing the reference frequencies for the experimental determination of CT (Table S2), it is clear how the amount of CT is related to the redshift of CT-sensitive bands in the near-IR region. Thus, the overestimation of CT and the need of implementing a noncanonical scaling factor (1.02 was the scaling factor used in this work to correctly reproduce the charge-sensitive frequencies) in order to obtain an acceptable match between spectra in the near-IR region at the PBE(D3BJ)/PAW level of the theory and the experimental results are deeply linked and intrinsic to the usage of PAWs. The electronic properties of the two molecular crystals were also investigated in as shown Figure 6; for both the Pery:F0 and Pery:F4 CT crystals, the band plot along high symmetry points and density of states (DOS) are reported. For both species, the DOS is dominated by the contribution of p orbitals, underlining once more the contribution of π-stacking interactions in the CT properties of Pery:F*n*TCNQ molecular crystals, confirming the need for better accounting the π-polarizability to model these systems. From the band plot, it can be seen how Pery:F0 is a direct semiconductor with a bandgap of 390 meV at Γ, while Pery:F4 has two significant bandgaps, one direct (223 meV at R) and one indirect (209 meV along X-R).

To further characterize the conduction properties, the phonon localization was investigated with the participation ratio (PR);[73,74] the PR goes from 1 to 1/*N* (*N* = number of atoms), indicating that with 1 mode all the atoms of the unit cell are moving with the same amplitude (typically rigid translations) and with 1/*N* modes only one atom is moving. The results for low frequency modes are displayed in Figure 7A for Pery-F0 and in Figure 7B for Pery-F4 (all PRs for each vibrational mode are reported in Tables S3 and S4). This analysis led to the presence of more delocalized modes for Pery:F4, which, however, are shifted toward higher frequencies, leading to a minor occupation probability. This is important as highly delocalized vibrations are associated with killer phonon modes[74,75] that are responsible for decreasing charge mobility and increasing the thermal molecular disorder; those vibrational modes are shown in Figure 7. In addition, the presence of highly delocalized phonons for Pery:F4 could promote the indirect semiconductor properties, making the transition along X-R permitted.

https://doi.org/10.1021/acs.jpcc.4c03470
J. Phys. Chem. C 2024, 128, 14046−14055

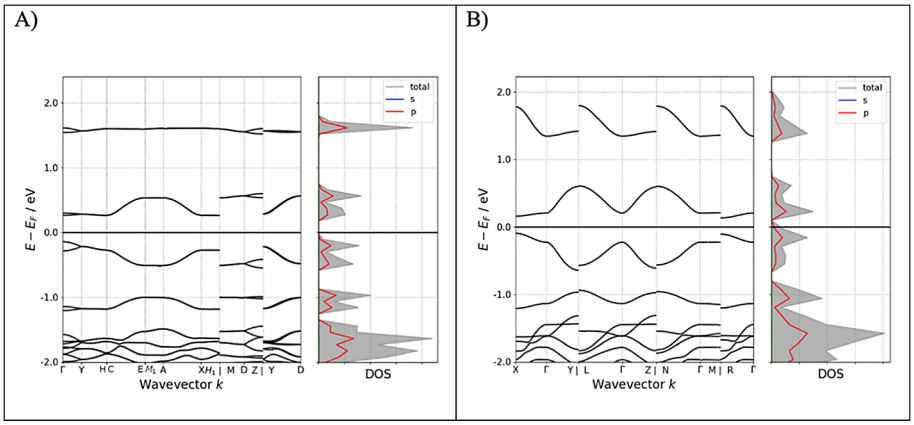

Figure 6. Band plot at high symmetry points and DOS, PBE(D3BJ)/PAW: A) Pery:F0 and B) Pery:F4.

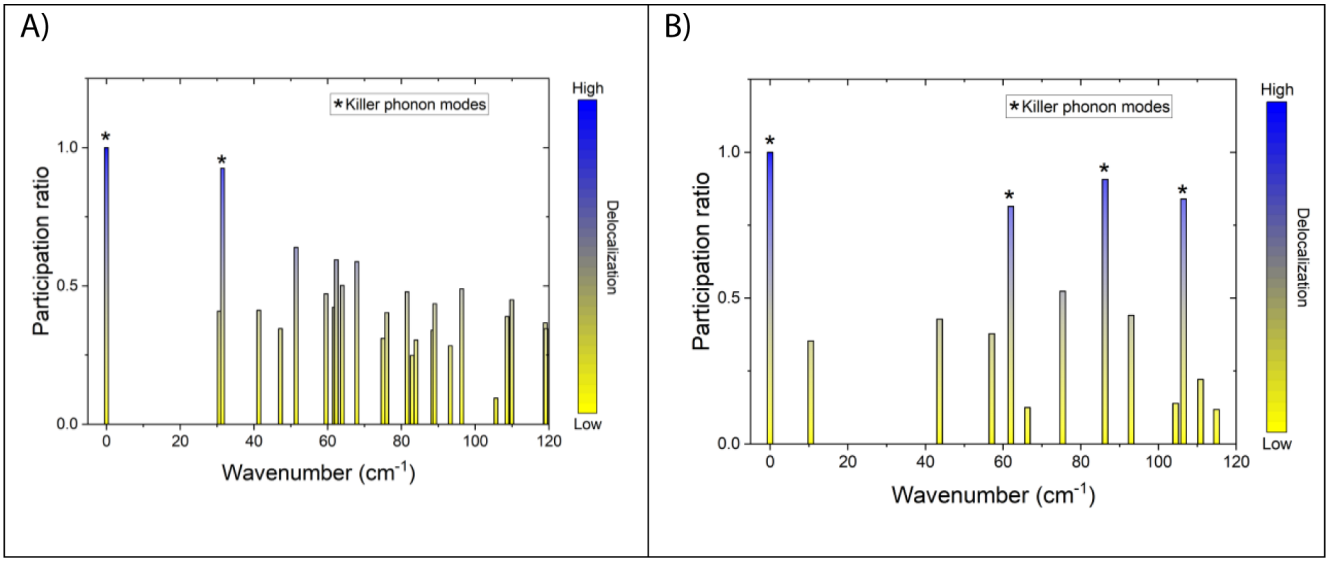

Figure 7. Participation ratio of low frequency vibrational modes: A) Pery:F0 and B) Pery:F4; highly delocalized phonons (i.e., killer phonon) are marked with an asterisk ("*").

CONCLUSION

Different theoretical strategies devoted to the quantitative estimation of the degree of charge-transfer in donor−acceptor organic complexes have been systematically considered in this paper, with a focus on the Pery:F*n*TCNQ (n = 0, 4) charge-transfer cocrystals. The CT values calculated with different strategies revealed marked differences. It must be noted that the widespread use of the PAW basis set in conjunction with the Bader population analysis led to unreliable values when dealing with CT π-complexes, even after the introduction of empirical dispersion corrections, while the rather straightforward approach of extracting a D−A dimer from the periodic CT crystal structure, and the subsequent evaluation of the CT degree within a localized orbital calculation framework proved to be a legit methodology if it was coupled with a careful choice of population analysis and level of theory. Specifically, CAM-B3LYP was a better performing functional tested in this work. Local hybrid and pure GGA functionals performed similarly to each other, overestimating the degree of CT, claiming the need for a long-range corrected hybrid functional to correctly describe the system. Furthermore, the influence of the basis set choice was investigated, finding an overestimation on the ionicity by adding diffuse functions (especially for Pople's split valence basis sets) and a negligible influence on the addition of polarization function. For PAW-based calculations, the problem lies in the overestimation of the ionicity of the system provided, which is caused by the exploitation of pseudopotentials (this is also reflected in the simulated Raman and IR spectra, where to compensate the ionicity overestimation, an empirical scaling factor is needed). In addition, the representation of π-polarizability (the importance of which was highlighted by DOS plots) is a known problem for both GGA and hybrid-GGA functionals, confirmed by the evidence that the best results, in close agreement with the experimental results, were obtained with a long-range corrected hybrid-GGA functional (CAM-B3LYP). The DDEC6 charge density decomposition scheme was the better performing population analysis, proving to be robust as exploited in various levels of the theory and giving acceptable results even with the use of plane-wave calculations. The application of this work has allowed us to confirm the CT of Pery:TCNQ to be 0.15 and not 0. Finally, from the band structure and phonon delocalization analysis, the semiconductor nature of each system was underlined, with a greater expected charge mobility for Pery:F4TCNQ due to the

https://doi.org/10.1021/acs.jpcc.4c03470
J. Phys. Chem. C 2024, 128, 14046−14055

presence of killer phonon modes at higher energies compared to Pery:TCNQ.

■ ASSOCIATED CONTENT

Supporting Information

The Supporting Information is available free of charge at https://pubs.acs.org/doi/10.1021/acs.jpcc.4c03470.

Comparison between experimental and calculated lattice parameters of Pery:F*n*TCNQ cocrystals (Table S1); summary of charge transfer sensitive modes of neutral and anion F*n*TCNQ (Table S2); calculated phonon frequencies, IR intensities, Raman activities, and participation ratio of Pery:F4TCNQ (Table S3); calculated phonon frequencies, IR intensities, Raman activities and participation ratio of Pery:TCNQ (Table S4); comparison between experimental Raman spectra (polarization averaged and nonaveraged) and the calculated one of Pery:TCNQ (Figure S1); experimental Raman spectra of Pery:TCNQ taken at different crystal orientations (Figure S2) (PDF)

Experimental structure of F4TCNQPerylene_1−1 (CIF)

Calculated structure of F4TCNQPerylene_1−1 (CIF)

Experimental structure of F0TCNQPerylene_1−1 (CIF)

Calculated structure of F0TCNQPerylene_1−1 (CIF)

■ AUTHOR INFORMATION

Corresponding Author

Claudio Fontanesi − *National Interuniversity Consortium of Materials Science and Technology (INSTM), Firenze 50121, Italy; Department of Engineering "Enzo Ferrari", (DIEF), University of Modena and Reggio Emilia, Modena 41125, Italy;* orcid.org/0000-0002-1183-2406; Email: claudio.fontanesi@unimore.it

Authors

Fabio Biffoli − *Department of Chemistry, "Ugo Schiff", University of Firenze, Firenze 50019, Italy; Materia Firenze Lab s.r.l., Gruppo Materia Firenze, Firenze 50018, Italy;* orcid.org/0000-0003-3330-6965

Davide Vanossi − *Department of Chemical and Geological Science, DSCG, University of Modena and Reggio Emilia, Modena 41125, Italy*

Elisabetta Venuti − *Department of Industrial Chemistry "Toso Montanari", INSTM-UdR Bologna, Bologna 40129, Italy;* orcid.org/0000-0003-3493-7953

Tommaso Salzillo − *Department of Industrial Chemistry "Toso Montanari", INSTM-UdR Bologna, Bologna 40129, Italy;* orcid.org/0000-0002-9737-2809

Marco Bonechi − *Department of Chemistry, "Ugo Schiff", University of Firenze, Firenze 50019, Italy;* orcid.org/0000-0003-0682-7976

Massimo Innocenti − *Department of Chemistry, "Ugo Schiff", University of Firenze, Firenze 50019, Italy; National Interuniversity Consortium of Materials Science and Technology (INSTM), Firenze 50121, Italy; Center for Colloid and Surface Science (CSGI), Firenze 50019, Italy*

Marco Pagliai − *Department of Chemistry, "Ugo Schiff", University of Firenze, Firenze 50019, Italy;* orcid.org/0000-0003-0240-161X

Complete contact information is available at: https://pubs.acs.org/10.1021/acs.jpcc.4c03470

Author Contributions

○F.B. and D.V. contributed equally.

Notes

The authors declare no competing financial interest.

■ ACKNOWLEDGMENTS

Financial support is gratefully acknowledged from the Ministry of University and Research (MUR), PRIN 2022 cod. 2022NW4P2T "From metal nanoparticles to molecular complexes in electrocatalysis for green hydrogen evolution and simultaneous fine chemicals production (FUTURO)", PI Dr. Fracesco Vizza, and from Fondazione di Modena, Fondo di Ateneo per la Ricerca Anno 2023, linea FOMO, Progetto AMNESIA, PI Prof. Claudio Fontanesi. Financial support is also gratefully acknowledged from Consorzio Interuniversitario Nazionale per la Scienza e Tecnologia dei Materiali (INSTM), fondi triennali: "INSTM21MOFONTANESI". Authors acknowledge also financial support by Fondazione CR Firenze: Fondazione per la Ricerca e l'Innovazione dell'Universitá degli Studi di Firenze and Confindustria Firenze, FABER4 project framework. T.S. thanks the Programma per Giovani Ricercatori "Rita Levi Montalcini" year 2020 (grant PGR20QN52R) of the Italian Ministry of University and Research (MUR) for the financial support. A project funded under the National Recovery and Resilience Plan (NRRP), Mission 04 Component 2 Investment 1.5—NextGenerationEU, call for tender no. 3277 dated 30/12/2021 (award number: 0001052 dated 23/06/2022) is also acknowledged.

■ REFERENCES

(1) Wiley-VCH Verlag GmbH & Co. *Organic Electronics: emerging Concepts and Technologies*, Cicoira, F.; Santato, C. Eds.; Wiley-VCH Verlag GmbH & Co. KGaA: Boschstr, Weinheim, Germany, Vol. *12*, pp 464, 2013.

(2) Vilan, A.; Yaffe, O.; Biller, A.; Salomon, A.; Kahn, A.; Cahen, D. Molecules on Si: Electronics with Chemistry. *Adv. Mater.* **2010**, *22* (2), 140−159.

(3) Hermerschmidt, F.; Choulis, S. A.; List-Kratochvil, E. J. W. Implementing Inkjet-Printed Transparent Conductive Electrodes in Solution-Processed Organic Electronics. *Adv. Mater. Technol.* **2019**, *4* (5), 1800474.

(4) Biscarini, F.; Coronado, E.; Painelli, A.; Yamashita, M. Materials for Molecular Electronics and Magnetism. *J. Mater. Chem. C* **2021**, *9* (33), 10521−10523.

(5) Bonechi, M.; Giurlani, W.; Stefani, A.; Marchetti, A.; Innocenti, M.; Fontanesi, C. Resorcinol Electropolymerization Process Obtained via Electrochemical Oxidation. *Electrochim. Acta* **2022**, *428*, 140928.

(6) King, B.; Lessard, B. H. Review of Recent Advances and Sensing Mechanisms in Solid-State Organic Thin-Film Transistor (OTFT) Sensors. *J. Mater. Chem. C* **2024**, *12* (16), 5654−5683.

(7) Chatterjee, O.; Roy, R.; Pramanik, A.; Dutta, T.; Sharma, V.; Sarkar, P.; Koner, A. L. Dynamic Self-Assembly of Photo-Reduced Perylene Diimide: Single-Component White Light Emission from Organic Radicals. *Adv. Opt. Mater.* **2022**, *10* (23), 2201187.

(8) Morvillo, P.; Diana, R.; Fontanesi, C.; Ricciardi, R.; Lanzi, M.; Mucci, A.; Tassinari, F.; Schenetti, L.; Minarini, C.; Parenti, F. Low Band Gap Polymers for Application in Solar Cells: Synthesis and Characterization of Thienothiophene-Thiophene Copolymers. *Polym. Chem.* **2014**, *5*, 2391.

(9) Holliday, S.; Donaghey, J. E.; McCulloch, I. Advances in Charge Carrier Mobilities of Semiconducting Polymers Used in Organic Transistors. *Chem. Mater.* **2014**, *26* (1), 647−663.

(10) Chatterjee, O.; Biswas, S.; Pramanik, A.; Silswal, A.; Paliwal, B.; Koner, A. L. Position and Number Do Matter: Tuning Room Temperature Phosphorescence in Bromo-1,8-Naphthalimides through H-Aggregation and Halogen Bonding. *Adv. Opt. Mater.* **2024**, *12* (15), 2303069.
(11) Goetz, K. P.; Vermeulen, D.; Payne, M. E.; Kloc, C.; McNeil, L. E.; Jurchescu, O. D. Charge-Transfer Complexes: New Perspectives on an Old Class of Compounds. *J. Mater. Chem. C* **2014**, *2* (17), 3065−3076.
(12) Shakya, S.; Khan, I. M. Charge Transfer Complexes: Emerging and Promising Colorimetric Real-Time Chemosensors for Hazardous Materials. *J. Hazard. Mater.* **2021**, *403*, 123537.
(13) Pramanik, A.; Biswas, S.; Pal, S.; Sarkar, P. Charge Transport and Transfer Phenomena Involving Conjugated Acenes and Heteroacenes. *Bull. Mater. Sci.* **2019**, *42* (3), 128.
(14) Henderson, J.; Masino, M.; Hatcher, L. E.; Kociok-Köhn, G.; Salzillo, T.; Brillante, A.; Raithby, P. R.; Girlando, A.; Da Como, E. New Polymorphs of Perylene: Tetracyanoquinodimethane Charge Transfer Cocrystals. *Cryst. Growth Des.* **2018**, *18* (4), 2003−2009.
(15) Zhang, C.; Wang, X.; Li, Y.; Sun, Y.; Zhang, Q. Spin in Organic Cocrystals. *Chem.-Eur. J.* **2023**, *29* (32), No. e202300481.
(16) Kaplan, I. G. *Theory of Molecular Interactions; Studies in physical and theoretical chemistry*; Elsevier: Amsterdam ; New York, 1986.
(17) Kitaigorodsky, A. *Molecular Crystals and Molecules*; Elsevier Science: Burlington, 2012.
(18) Oxford University Press. Fundamentals of Crystallography; *International Union of Crystallography texts on crystallography*, Giacovazzo, C., Ed.; Oxford University Press: Oxford, New York, 2002.
(19) Huang, Y.; Ning, L.; Zhang, X.; Zhou, Q.; Gong, Q.; Zhang, Q. Stimuli-Fluorochromic Smart Organic Materials. *Chem. Soc. Rev.* **2024**, *53* (3), 1090−1166.
(20) Salzillo, T.; Masino, M.; Kociok-Köhn, G.; Di Nuzzo, D.; Venuti, E.; Della Valle, R. G.; Vanossi, D.; Fontanesi, C.; Girlando, A.; Brillante, A.; Da Como, E. Structure, Stoichiometry, and Charge Transfer in Cocrystals of Perylene with TCNQ-F $_x$. *Cryst. Growth Des.* **2016**, *16* (5), 3028−3036.
(21) Biswas, S.; Pramanik, A.; Pal, S.; Sarkar, P. A Theoretical Perspective on the Photovoltaic Performance of S,N-Heteroacenes: An Even−Odd Effect on the Charge Separation Dynamics. *J. Phys. Chem. C* **2017**, *121* (5), 2574−2587.
(22) Voityuk, A. A. Electronic Coupling for Charge Transfer in Donor−Bridge−Acceptor Systems. Performance of the Two-State FCD Model. *Phys. Chem. Chem. Phys* **2012**, *14* (40), 13789.
(23) Gao, J.; Zhai, H.; Hu, P.; Jiang, H. The Stoichiometry of TCNQ-Based Organic Charge-Transfer Cocrystals. *Crystals* **2020**, *10* (11), 993.
(24) Anderson, M.; Ramanan, C.; Fontanesi, C.; Frick, A.; Surana, S.; Cheyns, D.; Furno, M.; Keller, T.; Allard, S.; Scherf, U.; Beljonne, D.; D'Avino, G.; Von Hauff, E.; Da Como, E. Displacement of Polarons by Vibrational Modes in Doped Conjugated Polymers. *Phys. Rev. Mater.* **2017**, *1* (5), 055604.
(25) Vanossi, D.; Cigarini, L.; Giaccherini, A.; Da Como, E.; Fontanesi, C. An Integrated Experimental/Theoretical Study of Structurally Related Poly-Thiophenes Used in Photovoltaic Systems. *Molecules* **2016**, *21* (1), 110.
(26) Vermeulen, D.; Zhu, L. Y.; Goetz, K. P.; Hu, P.; Jiang, H.; Day, C. S.; Jurchescu, O. D.; Coropceanu, V.; Kloc, C.; McNeil, L. E. Charge Transport Properties of Perylene−TCNQ Crystals: The Effect of Stoichiometry. *J. Phys. Chem. C* **2014**, *118* (42), 24688−24696.
(27) Solano, F.; Inaudi, P.; Abollino, O.; Giacomino, A.; Chiesa, M.; Salvadori, E.; Kociok-Kohn, G.; da Como, E.; Salzillo, T.; Fontanesi, C. Charge Transfer Modulation in Charge Transfer Co-Crystals Driven by Crystal Structure Morphology. *Phys. Chem. Chem. Phys.* **2022**, *24* (31), 18816−18823.
(28) Zhu, W.; Yi, Y.; Zhen, Y.; Hu, W. Precisely Tailoring the Stoichiometric Stacking of Perylene-TCNQ Co-Crystals towards Different Nano and Microstructures with Varied Optoelectronic Performances. *Small* **2015**, *11* (18), 2150−2156.
(29) Wu, H.-D.; Peng, H.-D.; Pan, G.-B. Precise Growth of Low-Dimensional pyrene·perylene·TCNQ Co-Crystals and Structure−Property Related Optoelectronic Properties. *RSC Adv.* **2016**, *6* (82), 78979−78983.
(30) Shokaryev, I.; Buurma, A. J. C.; Jurchescu, O. D.; Uijttewaal, M. A.; De Wijs, G. A.; Palstra, T. T. M.; De Groot, R. A. Electronic Band Structure of Tetracene−TCNQ and Perylene−TCNQ Compounds. *J. Phys. Chem. A* **2008**, *112* (11), 2497−2502.
(31) Salzillo, T.; Della Valle, R. G.; Venuti, E.; Kociok-Köhn, G.; Masino, M.; Girlando, A.; Brillante, A. Solution Equilibrium between Two Structures of Perylene-F2TCNQ Charge Transfer Co-Crystals. *J. Cryst. Growth.* **2019**, *516*, 45−50.
(32) Kumar, A.; Banerjee, K.; Ervasti, M. M.; Kezilebieke, S.; Dvorak, M.; Rinke, P.; Harju, A.; Liljeroth, P. Electronic Characterization of a Charge-Transfer Complex Monolayer on Graphene. *ACS Nano* **2021**, *15* (6), 9945−9954.
(33) Doan Truong, K.; Bandrauk, A. D. A New TCNQ Complex: (Perylene)3 TCNQ. *Chem. Phys. Lett.* **1976**, *44* (2), 232−235.
(34) Bandrauk, A. D.; Truong, K. D.; Carlone, C. Optical and Raman spectra of single crystals of perylene-TCNQ charge transfer complexes. *Can. J. Chem.* **1982**, *60* (5), 588−595.
(35) Solano, F.; Inaudi, P.; Chiesa, M.; Kociok-Köhn, G.; Salvadori, E.; Da Como, E.; Vanossi, D.; Malandrino, M.; Carmieli, R.; Giacomino, A.; Fontanesi, C. Spin Multiplicity and Solid-State Electrochemical Behavior in Charge-Transfer Co-Crystals of DBTTF/F4TCNQ. *J. Phys. Chem. C* **2021**, *125* (16), 8677−8683.
(36) Salzillo, T.; Marchetti, A.; Vejpravova, J.; Fanjul Bolado, P.; Fontanesi, C. Molecular Electrochemistry. An Overview of a Cross-Field: Electrochemistry/Spectroscopic/Theoretical Integrated Approach. *Curr. Opin. Electrochem.* **2022**, *35*, 101072.
(37) Kresse, G.; Furthmüller, J. Efficiency of Ab-Initio Total Energy Calculations for Metals and Semiconductors Using a Plane-Wave Basis Set. *Comput. Mater. Sci.* **1996**, *6* (1), 15−50.
(38) Kresse, G.; Furthmüller, J. Efficient Iterative Schemes for *Ab Initio* Total-Energy Calculations Using a Plane-Wave Basis Set. *Phys. Rev. B* **1996**, *54* (16), 11169−11186.
(39) Kresse, G.; Hafner, J. Norm-Conserving and Ultrasoft Pseudopotentials for First-Row and Transition Elements. *J. Phys.: Condens. Matter* **1994**, *6* (40), 8245−8257.
(40) Kresse, G.; Joubert, D. From Ultrasoft Pseudopotentials to the Projector Augmented-Wave Method. *Phys. Rev. B* **1999**, *59* (3), 1758−1775.
(41) Perdew, J. P.; Burke, K.; Ernzerhof, M. Generalized Gradient Approximation Made Simple [Phys. Rev. Lett. 77, 3865 (1996)]. *Phys. Rev. Lett.* **1997**, *78* (7), 1396−1396.
(42) Grimme, S.; Ehrlich, S.; Goerigk, L. Effect of the Damping Function in Dispersion Corrected Density Functional Theory. *J. Comput. Chem.* **2011**, *32* (7), 1456−1465.
(43) Togo, A.; Tanaka, I. First Principles Phonon Calculations in Materials Science. *Scr. Mater.* **2015**, *108*, 1−5.
(44) Skelton, J. M.; Burton, L. A.; Jackson, A. J.; Oba, F.; Parker, S. C.; Walsh, A. Lattice Dynamics of the Tin Sulphides SnS_2, SnS and Sn_2S_3: Vibrational Spectra and Thermal Transport. *Phys. Chem. Chem. Phys.* **2017**, *19* (19), 12452−12465.
(45) Frisch, M. J.; Trucks, G. W.; Schlegel, H. B.; Scuseria, G. E.; Robb, M. A.; Cheeseman, J. R.; Scalmani, G.; Barone, V.; Petersson, G. A.; Nakatsuji, H. *Gaussian 16, Revision B.01*, 2016.
(46) Manz, T. A.; Limas, N. G. Introducing DDEC6 Atomic Population Analysis: Part 1. Charge Partitioning Theory and Methodology. *RSC Adv.* **2016**, *6* (53), 47771−47801.
(47) Maintz, S.; Deringer, V. L.; Tchougréeff, A. L.; Dronskowski, R. LOBSTER: A Tool to Extract Chemical Bonding from Plane-wave Based DFT. *J. Comput. Chem.* **2016**, *37* (11), 1030−1035.
(48) Tang, W.; Sanville, E.; Henkelman, G. A Grid-Based Bader Analysis Algorithm without Lattice Bias. *J. Phys.: Condens. Matter* **2009**, *21* (8), 084204.

https://doi.org/10.1021/acs.jpcc.4c03470
J. Phys. Chem. C 2024, 128, 14046−14055

(49) Yu, M.; Trinkle, D. R. Accurate and Efficient Algorithm for Bader Charge Integration. *J. Chem. Phys.* **2011**, *134* (6), 064111.
(50) Lu, T.; Chen, F. Multiwfn: A Multifunctional Wavefunction Analyzer. *J. Comput. Chem* **2012**, *33* (5), 580−592.
(51) Yanai, T.; Tew, D. P.; Handy, N. C. A New Hybrid Exchange−Correlation Functional Using the Coulomb-Attenuating Method (CAM-B3LYP). *Chem. Phys. Lett.* **2004**, *393* (1−3), 51−57.
(52) Kendall, R. A.; Dunning, T. H.; Harrison, R. J. Electron Affinities of the First-Row Atoms Revisited. Systematic Basis Sets and Wave Functions. *J. Chem. Phys.* **1992**, *96* (9), 6796−6806.
(53) Miehlich, B.; Savin, A.; Stoll, H.; Preuss, H. Results Obtained with the Correlation Energy Density Functionals of Becke and Lee, Yang and Parr. *Chem. Phys. Lett.* **1989**, *157* (3), 200−206.
(54) Becke, A. D. Density-Functional Thermochemistry III. The Role of Exact Exchange. *J. Chem. Phys.* **1993**, *98* (7), 5648−5652.
(55) Adamo, C.; Barone, V. Toward Reliable Density Functional Methods without Adjustable Parameters: The PBE0Model. *J. Chem. Phys.* **1999**, *110* (13), 6158−6170.
(56) Ditchfield, R.; Hehre, W. J.; Pople, J. A. Self-Consistent Molecular-Orbital Methods IX. An Extended Gaussian-Type Basis for Molecular-Orbital Studies of Organic Molecules. *J. Chem. Phys.* **1971**, *54* (2), 724−728.
(57) Frisch, M. J.; Pople, J. A.; Binkley, J. S. Self-Consistent Molecular Orbital Methods 25. Supplementary Functions for Gaussian Basis Sets. *J. Chem. Phys.* **1984**, *80* (7), 3265−3269.
(58) Clark, T.; Chandrasekhar, J.; Spitznagel, G. W.; Schleyer, P. V. R. Efficient Diffuse Function-augmented Basis Sets for Anion Calculations. III. The 3-21+G Basis Set for First-row Elements, Li−F. *J. Comput. Chem.* **1983**, *4* (3), 294−301.
(59) Krishnan, R.; Binkley, J. S.; Seeger, R.; Pople, J. A. Self-Consistent Molecular Orbital Methods. XX. A Basis Set for Correlated Wave Functions. *J. Chem. Phys.* **1980**, *72* (1), 650−654.
(60) Dunning, T. H. Gaussian Basis Sets for Use in Correlated Molecular Calculations. I. The Atoms Boron through Neon and Hydrogen. *J. Chem. Phys.* **1989**, *90* (2), 1007−1023.
(61) Nanova, D.; Beck, S.; Fuchs, A.; Glaser, T.; Lennartz, C.; Kowalsky, W.; Pucci, A.; Kroeger, M. Charge Transfer in Thin Films of Donor−Acceptor Complexes Studied by Infrared Spectroscopy. *Org. Electron.* **2012**, *13* (7), 1237−1244.
(62) Girlando, A.; Painelli, A.; Pecile, C. Electron-Intramolecular Phonon Coupling in Regular and Dimerized Mixed Stack Organic Semiconductors. *Mol. Cryst. Liq. Cryst.* **1985**, *120* (1), 17−26.
(63) Painelli, A.; Girlando, A. Electron−Molecular Vibration (e−Mv) Coupling in Charge-Transfer Compounds and Its Consequences on the Optical Spectra: A Theoretical Framework. *J. Chem. Phys.* **1986**, *84* (10), 5655−5671.
(64) Kato, Y.; Matsumoto, H.; Mori, T. Absence of HOMO/LUMO Transition in Charge-Transfer Complexes of Thienoacenes. *J. Phys. Chem. A* **2021**, *125* (1), 146−153.
(65) Han, B.; Isborn, C. M.; Shi, L. Determining Partial Atomic Charges for Liquid Water: Assessing Electronic Structure and Charge Models. *J. Chem. Theory Comput.* **2021**, *17* (2), 889−901.
(66) Sotoudeh, M.; Baumgart, S.; Dillenz, M.; Döhn, J.; Forster-Tonigold, K.; Helmbrecht, K.; Stottmeister, D.; Groß, A. Ion Mobility in Crystalline Battery Materials. *Adv. Energy Mater.* **2024**, *14* (4), 2302550.
(67) Kodikara, M. S.; Stranger, R.; Humphrey, M. G. Long-Range Corrected DFT Calculations of First Hyperpolarizabilities and Excitation Energies of Metal Alkynyl Complexes. *ChemPhyschem* **2018**, *19* (12), 1537−1546.
(68) Alecu, I. M.; Zheng, J.; Zhao, Y.; Truhlar, D. G. Computational Thermochemistry: Scale Factor Databases and Scale Factors for Vibrational Frequencies Obtained from Electronic Model Chemistries. *J. Chem. Theory Comput.* **2010**, *6* (9), 2872−2887.
(69) Muniz-Miranda, F.; Pedone, A.; Muniz-Miranda, M. Raman and Computational Study on the Adsorption of Xanthine on Silver Nanocolloids. *ACS Omega* **2018**, *3* (10), 13530−13537.
(70) Krishnakumar, V.; Keresztury, G.; Sundius, T.; Seshadri, S. Density Functional Theory Study of Vibrational Spectra and Assignment of Fundamental Vibrational Modes of 1-Methyl-4-Piperidone. *Spectrochim. Acta, Part A* **2007**, *68* (3), 845−850.
(71) Muniz-Miranda, M.; Gellini, C.; Pagliai, M.; Innocenti, M.; Salvi, P. R.; Schettino, V. SERS and Computational Studies on MicroRNA Chains Adsorbed on Silver Surfaces. *J. Phys. Chem. C* **2010**, *114* (32), 13730−13735.
(72) Dobrowolski, M. A.; Garbarino, G.; Mezouar, M.; Ciesielski, A.; Cyrański, M. K. Structural Diversities of Charge Transfer Organic Complexes. Focus on Benzenoid Hydrocarbons and 7,7,8,8-Tetracyanoquinodimethane. *CrystEngcomm* **2014**, *16* (3), 415−429.
(73) Jiang, P.; Hu, S.; Ouyang, Y.; Ren, W.; Yu, C.; Zhang, Z.; Chen, J. Remarkable Thermal Rectification in Pristine and Symmetric Monolayer Graphene Enabled by Asymmetric Thermal Contact. *Applied Physics.* **2020**, *127*, 235101.
(74) Kamencek, T.; Zojer, E. Discovering Structure−Property Relationships for the Phonon Band Structures of Hydrocarbon-Based Organic Semiconductor Crystals: The Instructive Case of Acenes. *J. Mater. Chem. C* **2022**, *10* (7), 2532−2543.
(75) Schweicher, G.; D'Avino, G.; Ruggiero, M. T.; Harkin, D. J.; Broch, K.; Venkateshvaran, D.; Liu, G.; Richard, A.; Ruzié, C.; Armstrong, J.; Kennedy, A. R.; Shankland, K.; Takimiya, K.; Geerts, Y. H.; Zeitler, J. A.; Fratini, S.; Sirringhaus, H. Chasing the "Killer" Phonon Mode for the Rational Design of Low-Disorder, High-Mobility Molecular Semiconductors. *Adv. Mater.* **2019**, *31* (43), 1902407.

https://doi.org/10.1021/acs.jpcc.4c03470
J. Phys. Chem. C 2024, 128, 14046−14055